Exp Fluids (2006) 41:803–812
DOI 10.1007/s00348-006-0205-y

RESEARCH ARTICLE

The effect of photobleaching on PLIF

L. G. Larsen · J. P. Crimaldi

Received: 27 April 2006 / Revised: 19 July 2006 / Accepted: 21 August 2006 / Published online: 15 September 2006

Abstract Organic dyes commonly used for planar laser-induced fluorescence (PLIF) are susceptible to photobleaching under laser excitation. Previous work has shown that photobleaching can induce significant errors in laser-induced fluorescence measurements made with single-point techniques. This paper presents an analytical model and experimental results that quantify the extent of photobleaching in the more common planar configuration of the technique. Experimental results for two common dyes, fluorescein and Rhodamine 6G, agree well with analytical predictions for typical PLIF parameters. Results indicate that even dyes such as fluorescein that have large photobleaching constants can be used with little error in many PLIF experiments.

1 Introduction

Laser-induced fluorescence (LIF) is commonly used to measure scalar concentrations and fluxes in fluid flows where a fluorescent dye is used as the scalar surrogate. The dye is excited by a laser, inducing fluorescence such that the emitted light can be quantified with a photomultiplier tube or a CCD chip in a digital camera. Under appropriate conditions, the fluorescence is proportional to the concentration of dye present in the area of interest (Koochesfahani and Dimotakis 1985).

L. G. Larsen · J. P. Crimaldi (✉)
The University of Colorado, 428 UCB,
Boulder, CO 80309-0428, USA
e-mail: John.Crimaldi@colorado.edu

In fluid mechanics, the LIF technique is commonly used to measure scalar concentrations (Coppeta and Rogers 1994; Crimaldi and Koseff 2001), temperatures (Coppeta and Rogers 1995; Sakakibara and Adrian 1999; Hishida and Sakakibara 2000), or velocities (Borg et al. 1985) in a laboratory flow field. Depending on the optical setup, LIF can be used to determine relative concentrations at a single point (Durst and Schmitt 1984; Crimaldi 1997), along a line (Koochesfahani 1984; Westblom and Svanberg 1985; Brungart et al 1991), within a plane (Houcine et al. 1996; Karasso and Mungal 1997), or within a three-dimensional volume (Prasad and Sreenivasan 1990; Goldstein and Smits 1994; Tian and Roberts 2003). The most common implementation of LIF in fluid mechanics is planar laser-induced fluorescence (PLIF). In PLIF, a laser sheet is created within the flow, exciting the dye and causing it to fluoresce. Images of the spatial distribution of fluorescence intensity can be processed into calibrated concentrations, as described in Sect. 3.1. Applications of PLIF are multifold, including determining concentration statistics within a turbulent boundary layer (Crimaldi and Koseff 2001; Crimaldi et al. 2002; Webster et al. 2003; Mead et al. 2003), understanding mixing and dispersion processes at boundary layers (Houcine et al. 1996; Munsterer and Jahne 1998) or in turbulent jets (Catrakis and Dimotakis 1996; Webster et al. 2001), and assessing transport processes within the flow (Lemoine et al. 1999; Cowen et al. 2001). In this paper, we examine the effect of photobleaching on the accuracy of the PLIF technique.

When a dye molecule absorbs an incident photon, it is promoted to the singlet excited state, which is unstable. Once in the singlet excited state, the mole-

cule may follow one of the three different pathways. Typically, the dye will return to the ground state through emission of a photon in the process of fluorescence. Other pathways available to the excited molecule are a radiationless, internal conversion back to the ground state or conversion to the triplet state through intersystem crossing. Dye molecules in the triplet state are vulnerable to physical or chemical quenching, which returns the molecule to the ground state, or to photobleaching, which irreversibly converts the dye molecule to a colorless leucocompound that is no longer able to fluoresce when exposed to further photon flux (Oster and Adelman 1956; Guilbault et al. 1990; Song et al. 1995, 1996).

At low excitation intensities, dye concentrations and time exposure to the exciting light source, conversion of dye in the singlet excited state to the triplet state is minimal, and the fluorescence observed through PLIF is proportional to the concentration of dye present in the imaged area for a spatially uniform pH and temperature (Walker 1987). However, at sufficiently long exposure times or intense excitation, photobleaching becomes significant, thereby leading to a lower fluorescence for the given concentration of dye in the imaged area and an underestimate of measured dye concentrations. Different dyes have different susceptibilities to photobleaching; fluorescein, popular because of its low cost, low temperature and pH dependence, high quantum yield (Magde et al. 2002), high solubility in water, low toxicity (Smart and Laidlaw 1977) and high molar absorption at the 488 nm line of the Ar–I laser is particularly susceptible (Crimaldi 1997).

Various researchers have examined the photobleaching process in common dyes. Many of these researchers (Imamura and Koizumi 1955; Song et al. 1995, 1997) noticed that for low concentrations of dye and relatively low incident light intensity, photobleaching occurs as a first-order process with a rate proportional to the incident light intensity (Koochesfahani 1984). Crimaldi (1997) adapted this formulation into an analytical model of photobleaching for point LIF geometries. No previous studies, however, have directly examined the extent of photobleaching on the more ubiquitous PLIF configuration, which differs significantly in its geometry. This study is designed to predict the photobleaching error associated with a particular dye and experimental PLIF configuration. Its aims are to:

1. Develop an analytical model based on the first order kinetics of Koochesfahani (1984) that describes the extent of photobleaching in a PLIF system for single and multiple laser scans.
2. Experimentally test the validity of the analytical model.
3. Compare photobleaching in the two different implementations of PLIF: the line-scan method and the cylindrical lens method.

2 Analytical

2.1 Fluorescence equations for PLIF geometry

In PLIF, the laser sheet used to illuminate dye concentrations within a plane is commonly created through one of the two different techniques. The line-scan (LS) method (Crimaldi and Koseff 2001; Stapountzis et al. 1992; Hishida and Sakakibara 2000; Webster et al. 2003) employs a galvanometer or rotating mirror, which scans a laser beam with circular cross-section across the measurement area, as seen in Fig. 1. In the cylindrical lens (CL) method (Coolen et al. 1999; Houcine et al. 1996; Coppeta and Rogers 1995, 1994; Das et al. 2005), a stationary beam passes through a cylindrical lens and is then directed into the measurement volume. As shown in Fig. 2, the cylindrical lens expands the beam along one dimension, creating a Gaussian sheet. Still other workers (Sakakibara and Adrian 1999) employ a combination of the CL and LS techniques, using a galvanometer or rotating mirror to slowly sweep a beam that has been expanded into a sheet with a cylindrical lens through the image area.

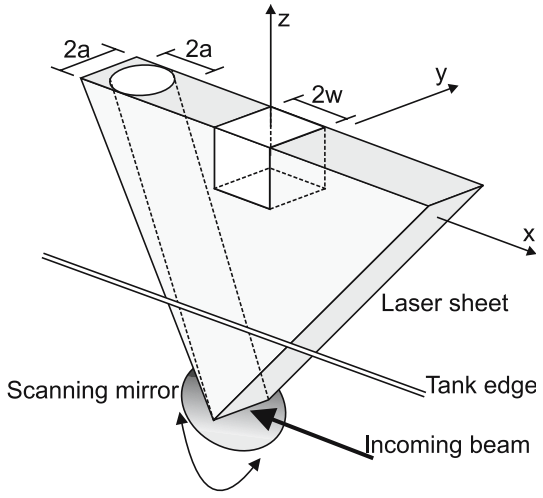

Fig. 1 Establishment of laser sheet and pixel geometries in the LS–PLIF technique. The Cartesian coordinate system employed in the analytical model is defined based on the pixel geometry, which is, in turn, defined by sheet dimensions. Variables used in the analytical model are also defined in the diagram. The half-width of the pixel is defined as w, whereas the beam radius is defined as a

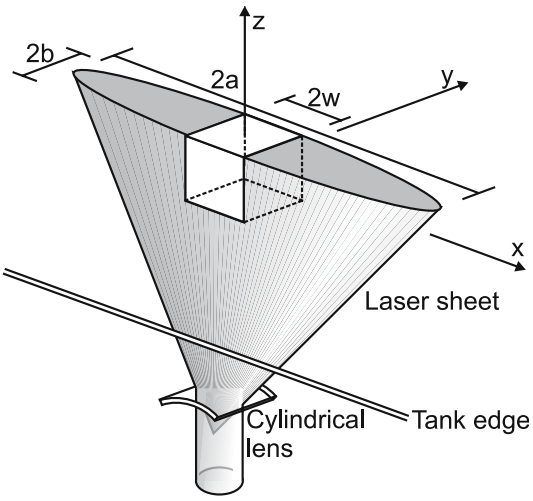

Fig. 2 Establishment of laser sheet and pixel geometries in the CL–PLIF technique. As in the LS case, w is the pixel half-width, while a and b are the long and short axes, respectively, of the elliptical cross-section of the laser sheet

Despite their differences, the LS and CL methods can be modeled similarly. Namely, the CL method can be modeled as an LS process for a beam with an elliptical cross-section and a relative flow velocity, U, that equals the mean flow velocity. Relative flow velocity for the LS method, in contrast, is calculated by subtracting the mean flow velocity from the laser scan velocity.

In the PLIF configuration depicted in Fig. 2, the laser is operated in TEM_{00} mode, so the intensities in the cross-section of the beam can be described by a two-dimensional Gaussian method. Let a and b be the e^{-2} beam radii along the long and short axes of the elliptical cross-section. The PLIF system images a small fluid volume (hereafter referred to as the pixel volume) within the laser scan onto a single CCD pixel. Fluorescence intensity acquired by the CCD chip is modeled for each pixel individually. An x, y, z Cartesian coordinate system with the origin at the center of the imaged pixel is established, and x, y, and z are normalized by b to x^*, y^*, and z^*. We define the pixel width, thickness, and height to be the lengths of the pixel in the x-, y-, and z- directions, respectively (see Figs. 1, 2). The imaged pixel thickness (defined as the e^{-2} thickness of the pixel volume) is $2b$. In addition, time t is normalized by the total amount of time required for the laser to execute a complete scan over the pixel, as described in Sect. 2.2. The relative intensity value measured by the CCD camera for each pixel is the local instantaneous fluorescence, integrated over pixel volume and exposure time. This total fluorescence is normalized so that the value is unity when photobleaching is nonexistent and zero when complete bleaching occurs (Crimaldi 1997):

$$F^* = \iiint I^*(x^*, y^*, t^*) C^*(x^*, y^*, t^*) \mathrm{d}x^* \mathrm{d}y^* \mathrm{d}t^*, \qquad (1)$$

where local laser intensity, I, and unbleached dye concentration, C, are normalized so that the total power within the beam cross-section and total initial concentration prior to photobleaching, respectively, are unity. It is assumed that laser intensity and concentration within each pixel are invariant with z. This assumption is satisfied when Lambert–Beer's Law beam attenuation over the height of the pixel is sufficiently small and when vertical differences in beam intensity due to the sweep arc of the beam or beam spreading from a focal point are minimal. Violations of the assumption of z-direction invariance will lead to an underestimate or overestimate of the extent of photobleaching, depending on whether the incident laser intensity at the top or bottom of the pixel is employed in calculations. Choosing small pixel heights, low dye concentrations, and pixel locations centered on the focus of the beam and far from the pivot of the scanning mirror minimizes errors due to such violations. For each pixel of interest, Lambert–Beer's Law and beam spreading calculations should be applied in advance to determine the appropriate laser power and beam dimensions to use in photobleaching calculations.

2.2 Modeling laser intensity

Since the laser intensity over time can be modeled by a simple translation of the two-dimensional Gaussian beam intensity profile, it is assumed that the distance between the scanning mirror and the center of the pixel of interest is large enough that angular tilting of the beam due to the motion of the scanning mirror can be neglected, which is exactly true at the center column of the image (see Fig. 3). Then, intensity, or energy flux per unit time (W m^{-2}), can be written as

$$I(x^*, y^*, t^*) = \frac{2P}{\pi ab} \exp\left\{ -2\left[\frac{b^2}{a^2}(x^* - d^*)^2 + y^{*2} \right] \right\}, \qquad (2)$$

where d^* is the time-varying distance between the beam and pixel centers, normalized by b. P is the total laser power in the beam cross-section at the location of the pixel. The pixel width is $2w$, as seen in Figs. 1 and 2, and time is normalized so that at $t^* = 0$ the beam center is located one beam radius a up-scan of the pixel edge and that, at $t^* = 1$, the beam center is one beam radius down-scan of the pixel. In other words,

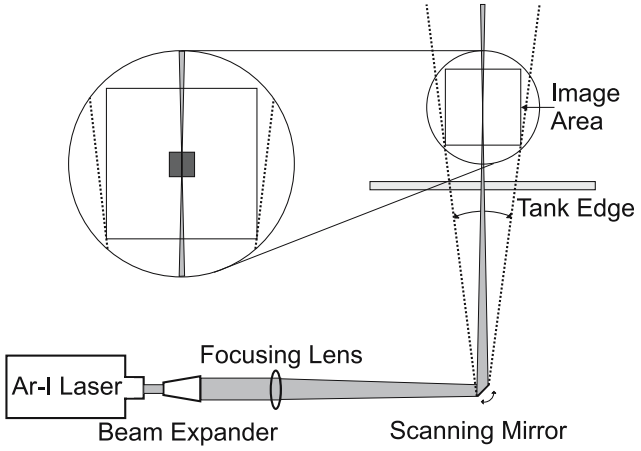

Fig. 3 Geometry for PLIF image acquisition. The CCD camera used to capture the image would be positioned above the plane of the figure. *Inset* The *darkly shaded square* represents the suite of pixels averaged in the acquisition of photobleaching data. This group of pixels is located directly above the center axis of the scanning mirror

$d = -\frac{(w+a)}{b}$ when $t^* = 0$ and $d^* = \frac{w+a}{b}$ when $t^* = 1$ for a single laser scan. The normalized time t^* is then

$$t^* = \frac{\dot{s}t}{2(w+a)}, \tag{3}$$

2.3 Modeling dye concentration

Based on the first order photobleaching kinetics reported by Koochesfahani (1984), Crimaldi (1997) derives the equation for the unbleached concentration of dye remaining at time t after exposure to a time-dependent excitation intensity:

$$C(t) = C_0 \exp\left[\frac{-Q_b\sigma}{h\nu}\int_{t_0}^{t} I(\tilde{t})\mathrm{d}\tilde{t}\right], \tag{6}$$

where C_0 is the concentration of the dye at time t_0, $\tilde{t}$ is a variable of integration, Q_b is the number of dye molecules bleached per absorbed photon, σ is the absorption cross-section of the dye, ν is the frequency of excitation light, and h is Planck's constant. This equation assumes first-order photobleaching kinetics, which is valid when a dye–oxygen mechanism of photobleaching dominates (Song et al. 1997). To apply this equation to the geometry of a PLIF pixel volume, $C(t)$ is normalized by dividing the right-hand side of the equation by C_0, and Eq. 2 is integrated from zero to t^*. When the term in front of the integral is nondimensionalized, Eq. 6 becomes

$$C^*(x^*,y^*,t^*) = \exp\left\{\frac{Q_b\sigma P}{h\nu b\dot{s}\sqrt{2\pi}}\exp[-2y^{*2}]\left[\mathrm{erf}\left(\frac{\sqrt{2}b}{a}\left(x^* + \frac{w+a-2(w+a)t^*}{b}\right)\right) - \mathrm{erf}\left(\frac{\sqrt{2}b}{a}\left(x^* + \frac{w+a}{b}\right)\right)\right]\right\}. \tag{7}$$

where $\dot{s}$ is the linear scan rate of the beam relative to the fluid. When S is the linear scan rate of the beam and U is the fluid velocity component in the x-direction, $\dot{s} = |S - U|$. Note that $S = r\dot{\theta}$, where r is the distance between the scanning mirror and the center of the pixel and $\dot{\theta}$ is the angular scan rate of the mirror. In the CL method, $S = 0$, and $\dot{s} = U$.

Following the convention of Crimaldi (1997), I^* is normalized so that

$$\iint I(x^*,y^*,t^*)\mathrm{d}x^*\mathrm{d}y^* = 1. \tag{4}$$

Solving Eq. 4 and applying the definition of d^*, the normalized intensity can be written as

$$I^*(x^*,y^*,t^*) = \frac{2b}{\pi a}\exp\left\{-2\left[\frac{b^2}{a^2}\left(x^* + \frac{w+a-2(w+a)t^*}{b}\right)^2 + y^{*2}\right]\right\}. \tag{5}$$

Notably, the coefficient within the exponential is equivalent to Crimaldi's (1997) nondimensional photobleaching parameter B, with $\dot{s}$ replacing u:

$$B = \frac{Q_b\sigma P}{h\nu b\dot{s}\sqrt{2\pi}}. \tag{8}$$

Now that Eq. 7 has been specified, the normalized fluorescence intensity expected for a pixel can be solved. Equations 1, 5, and 7 are numerically integrated for $-1 \le y^* \le 1, -\frac{w}{b} \le x^* \le \frac{w}{b}$, and $0 \le t^* \le 1$. This analysis is also extended to the case in which a dye parcel is exposed to multiple, simultaneous scans, in which the upper bound on t^* is the total number of scans.

2.4 Incomplete traverses

The model above allows for calculation of the photobleaching after one complete pass through the Gauss-

ian sheet in the CL technique or after a complete laser scan in the LS technique. While the rapid scan velocities employed in LS–PLIF allow the assumption that the parcel remains within the imaged plane for the duration of the scan to be reasonable, it is unlikely that the fluid parcel in the CL–PLIF technique will remain within the sheet as it flows from the left edge to the right edge. For typical laboratory flows, the solution to the photobleaching equations presented above would overestimate the actual extent of photobleaching observed within a pixel. Thus, a second solution is derived in which the fluid parcel incompletely traverses the Gaussian sheet.

As the Gaussian sheet is stationary within the flow, the origin of the x, y, z coordinate system is naturally chosen as the center of the Gaussian, and pixel boundaries are defined with respect to this origin. Due to the stationarity of the sheet, d^* in Eq. 2 is zero. To solve for unbleached dye concentration at a particular location, we use an alternative to Eq. 6, also given by Crimaldi (1997) for the case in which the dye parcel moves through a spatially varying excitation intensity field:

$$C(x) = C_0 \exp\left[\frac{-Q_b\sigma}{h\nu U}\int_{x_0}^{x} I(\tilde{x})\mathrm{d}\tilde{x}\right], \tag{9}$$

where $\tilde{x}$ is a variable of integration. The lower limit of integration, x_0, is the starting point of the fluid parcel's path within the sheet, or $x - U\theta$, where θ is the amount of time the parcel has spent within the sheet. For convenience, we choose a different time normalization scheme so that the amount of nondimensional time required for a fluid parcel to pass through one pixel is unity:

$$\theta^* = \frac{U}{2w}\theta. \tag{10}$$

Solving the integral and normalizing by C_0, Eq. 9 becomes

$$C^*(x^*, y^*, \theta^*) = \exp\left\{B\exp(-2y^{*2})\left[\mathrm{erf}\left(\frac{\sqrt{2}b}{a}\left(x^* - \frac{2w\theta^*}{b}\right)\right) - \mathrm{erf}\left(\frac{\sqrt{2}b}{a}x^*\right)\right]\right\}. \tag{11}$$

To solve Eq. 1, it is assumed that all fluid parcels passing through the pixel originated in the sheet at the same time (fluid parcels have the same initial path length). Then, the quantity $I^*(x^*,y^*)C^*(x^*,y^*,z^*)$ is integrated over the spatial area of the pixel and from the number of pixels the fluid parcel has traversed within the sheet at the start of the exposure to the number of pixels traversed in the sheet at the end of the exposure in θ^*.

Note that Eq. 11 in not appropriate for the special case in which U is zero and the fluid parcel is illuminated by a CL pulse of duration T. In this case, Eq. 6 simplifies because the incident laser intensity does not vary with time during the pulse duration (i.e., d^* is time-invariant). Equation 9 becomes

$$C^*(x^*, y^*, T) = \exp\left\{\frac{-2Q_b\sigma PT}{h\nu ab\pi}\exp\left[-2\left(\frac{b^2}{a^2}(x^* - d^*)^2 + y^{*2}\right)\right]\right\}. \tag{12}$$

2.5 Analytical model results

Figure 4 shows the results after integrating Eq. 1 for a single laser scan and a continuum of B-values, using the LS technique. The shape of the photobleaching curve remains unchanged for different values of pixel width. For low values of B (corresponding to low laser intensity and/or high net scan rate) the effects of photobleaching are negligible, but photobleaching increases nonlinearly as B increases (P increases and/or $\dot{s}$ decreases). If F^* is to remain within one percent of its unbleached value, B must be smaller than 0.014. The nondimensional photobleaching curve for the LS technique is plotted alongside the curve for a typical application of the CL technique, in which Eq. 11 is integrated for a pixel at the center of the image, a path length (p) of 1 cm, a laser sheet 10 cm wide by 0.01 cm thick, and a continuum of B-values. The total nondimensional exposure time for the generation of this curve is unity. The shape of the curve varies strongly with path length and pixel position and weakly with sheet dimensions. The position of this curve above the photobleaching curve for the LS technique at most values of B indicates that, for a given B, the amount of photobleaching expected from one scan of the laser in the LS technique is greater than that induced by the passage of dye through 1 cm of the CL laser sheet under these conditions. Recall from the definition of B,

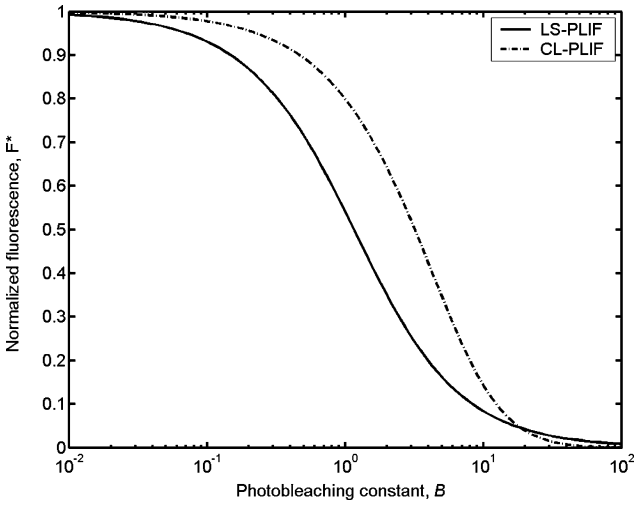

Fig. 4 Normalized fluorescence, F^*, versus the photobleaching parameter, B, for different implementations of LIF. The curve for the LS–PLIF configuration was obtained for a pixel in the center column of the image after exposure to a single passage of the laser beam, while the curve for the CL–PLIF configuration was obtained for a pixel in the same location after the fluid parcel comprising that pixel passed through a length of 1 cm within a laser sheet 10 cm wide by 0.01 cm thick

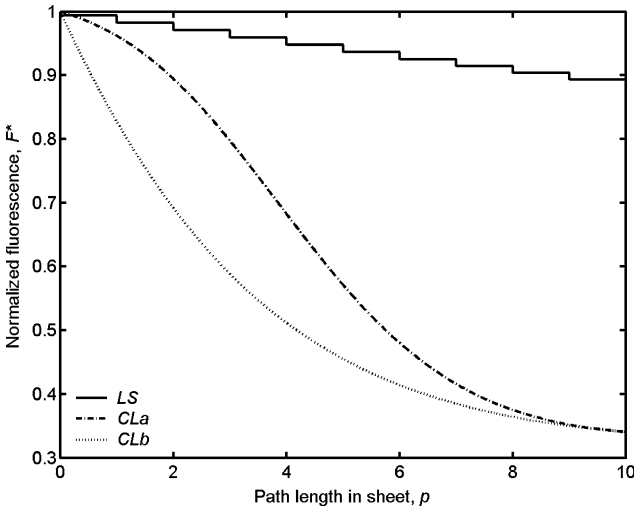

Fig. 5 Normalized fluorescence, F^*, versus path length, p, fluid parcel has traveled within the laser sheet for the CL and LS implementations of PLIF under the conditions provided in Table 1. Due to sheet nonuniformities in the CL implementation, the photobleaching experienced for a particular path length varies for different pixel locations within the laser sheets, so both a best-case and worst-case photobleaching scenario are presented for the CL technique. In the best-case scenario (CLa), the pixel is located at the downstream edge of the laser sheet, while the worst-case scenario (CLb) provides the photobleaching occurring in a pixel at the end of a fluid parcel path length centered on the laser sheet Gaussian

however, that since the laser scan velocity employed in the LS technique is typically much greater than the flow velocity of the fluid, B will typically be much smaller in the LS technique than in the CL technique. For example, in the common PLIF configuration outlined in Table 1, B is 0.0082 for the LS technique and 0.82 for the CL technique. Whether this lower B translates into less photobleaching requires further examination, detailed below.

Figure 5 compares the photobleaching that would be experienced in LS and CL implementations of the PLIF configuration outlined in Table 1. In the curve presented for the LS configuration, generated using the model for multiple laser scans, F^* decreases with p in a stepwise fashion due to the discrete nature of the laser scans across the image. For this example, the beam is scanned at a frequency of 10 Hz, which is at the high-frequency end of the range put into practice in the laboratory. The first scan is assumed to occur when the fluid parcel enters the sheet area, and location of the pixel at which photobleaching is evaluated translates with the fluid parcel. In the CL technique, laser intensity varies in a Gaussian form across the sheet, and thus, photobleaching is strongly dependent on pixel location. The least amount of photobleaching occurs at the edges of the sheet, where laser intensity is low, while the greatest amount occurs at the center. Curve CLa in Fig. 5 presents the photobleaching that would be experienced by a fluid parcel terminating its path through the light sheet at the downstream edge of the sheet. Due to the pixel location at the edge of the Gaussian, this curve provides a best-case estimate of the photobleaching occurring within the CL implementation of PLIF. For low values of p, the curve decreases with a shallow slope, due to the low intensities at the edge of the Gaussian. As the path length extends into the center region of the image, where laser intensities are high, F^* decreases with a steeper slope. Then, as the path length extends into the low-intensity upstream portion of the Gaussian, the slope of the F^* versus p curve again decreases.

Curve CLb in Fig. 5 presents the photobleaching that would be experienced by a fluid parcel with path length centered on the Gaussian. Thus, at low p, F^* is reported for a pixel near the center of the image, while at high p, F^* is reported for a pixel near the downstream edge of the image. The slope of this curve decreases with increasing p as the path of the fluid parcel

Table 1 PLIF configuration used in text example

Fluid velocity, U	10 cm/s
Image size	10 cm
Number of pixels per column	1,000
Integration time	10 ms
Image acquisition frequency	10 Hz

extends into the tails of the Gaussian. This curve provides a worst-case estimate of the photobleaching occurring within the CL implementation of PLIF.

From Fig. 5, it is evident that for the PLIF configuration outlined in Table 1, the LS technique results in significantly less photobleaching than the CL technique for path lengths greater than 0.22 cm. Below 0.22 cm, curve CLa features higher F^* values than curve LS, but it is only below path lengths of 0.02 cm that curve CLb rises above curve LS. Differences between the three curves are so slight for path lengths lower than 0.22 cm, though, that practically, the dye would experience very similar extents of photobleaching in each of the implementations at small path lengths within the laser sheet. For both configurations, as path length increases, the value of B required to maintain negligible photobleaching decreases.

3 Experimental

3.1 Materials and methods

The goal of the experimental portion of this analysis was to validate the first-order analytical model that was developed for PLIF geometry for low laser intensities and dye concentrations. Experiments were performed in a 5.5-gallon glass tank filled with a well-mixed dye solution. The 488 nm line of an argon-ion laser was used as the exciting light source. The laser beam was expanded and then focused such that the beam waist corresponded with the measurement location. The e^{-2} beam waist diameter was 0.45 mm, as determined by fitting a Gaussian to transects of images of the beam. A scanning mirror directed the focused beam into the tank to create the light sheet shown in Fig. 3. A CCD camera captured the fluorescence emitted from the laser light sheet. Image intensity from a 200 × 200 square of pixels at the center of the image area was averaged to obtain F^*, and five images were used to obtain each point on the nondimensional photobleaching curve. Raw images (A) were corrected for camera dark response (D), exposure time/scan rate, and laser intensity to obtain concentrations in accordance with the following algorithm, based on Crimaldi and Koseff (2001):

$$C_n = \alpha(A_n - D_n)\left(\frac{\dot{s}_n}{I_n}\right), \tag{13}$$

where α is a spatially-varying constant of proportionality that reflects variations in pixel gain, dark response, lens vignette, and nonuniformities in the laser scan. Here, the "n" subscript refers to the experimental conditions used to generate each point. F^* is obtained by normalizing C_n by C_0, where C_0 is the dye concentration in the negligible photobleaching condition, obtained by progressively reducing the photobleaching constant B until raw fluorescence, corrected for exposure time and intensity, becomes invariant.

To compare experimental photobleaching results to analytical results, F^* was obtained under the aforementioned configuration for B values ranging from less than 10^{-3} to greater than 10^{0}. B is varied by adjusting the integration time while maintaining a constant laser power of 1.5 W. Corresponding values of B and F^* form points on the nondimensional photobleaching curve. Finally, the experimental photobleaching curve was then fit to the analytical photobleaching curve by adjusting $Q_b\sigma$, as detailed below.

3.2 Experimental results

The experimental photobleaching curves obtained using two different initial fluorescein dye concentrations (20 and 200 ppb) and a Rhodamine 6G dye concentration of 5 ppb are plotted against the analytical photobleaching curve in Fig. 6. Experimental results produce good agreement to the analytical curve for values of the photobleaching constant less than 0.2. $Q_b\sigma$ was optimized by applying a least-squares minimization of error procedure to the points on this por-

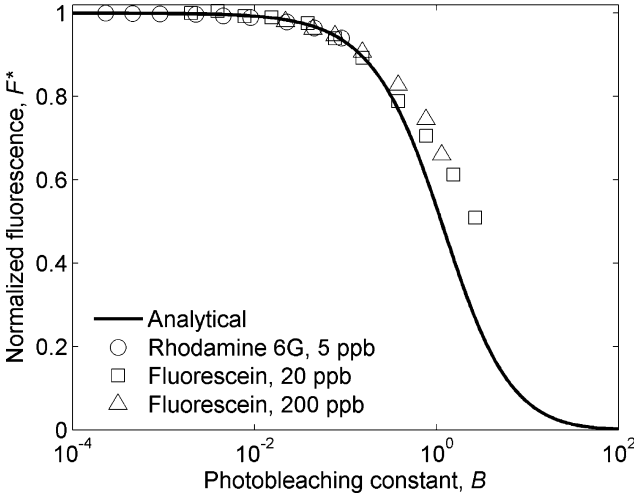

Fig. 6 Experimental versus analytical normalized photobleaching curves, generated under a single scan of the laser in the LS–PLIF configuration. The analytical curve results from integration of equation 1, and experimental results are reported for Rhodamine 6G (5 ppb) and fluorescein (20 and 200 ppb). $Q_b\sigma$ values are 8.2×10^{-22} cm^2 for Rhodamine 6G and 1.4×10^{-20} cm^2 for fluorescein

tion of the curve. The best-fit values of $Q_b\sigma$ were determined to be 1.4×10^{-20} cm^2 for fluorescein and 8.2×10^{-22} cm^2 for Rhodamine 6G, which result in R^2 values of 0.98 for both dyes. These $Q_b\sigma$ values are within the same order of magnitude as the values reported by Crimaldi (1997). Experimental photobleaching curves obtained using three different initial dye concentrations are statistically indistinguishable, verifying that the rate constant of photobleaching is not dependent upon concentration and upholding the assumption that the Lambert–Beer's Law attenuation of incident light is negligible.

As seen in Fig. 6, at high values of B (>0.2), the experimental photobleaching curve begins to deviate from the analytical curve; less photobleaching is observed than predicted. Experiments suggest that this deviation resulted neither from out-of-plane motions during the exposure nor limited diffusion of dissolved oxygen to the image plane with respect to the rate of occurrence of the dye-oxygen mechanism that is thought to dominate photobleaching kinetics (Song et al. 1996). This deviation, however, occurs only at impractically long exposures, which, if employed, would result in substantial error due to fluid motion and factors other than photobleaching.

4 Discussion and conclusions

Although Crimaldi (1997) thoroughly analyzed the extent of photobleaching in single-point LIF configurations, this paper presents the first comprehensive study of the extent of photobleaching in the more common PLIF configuration. Model results indicate that for typical values of B employed in PLIF, photobleaching is not likely to be significant, even for dyes with large values of $Q_b\sigma$ such as fluorescein. Photobleaching increases to significant levels with multiple scans, but in turbulent flow, it is unlikely that a dye parcel will remain within the flow for more than one scan. In the CL implementation of PLIF, photobleaching is more significant for a complete pass through the expanded beam than for a comparable LS implementation, reflecting a B value that is nearly two orders of magnitude higher than that for a comparable LS configuration, due to the longer time of illumination. However, it is similarly unlikely in the CL implementation that a fluid parcel in a turbulent flow will remain within the illuminated area long enough to experience significant bleaching. For shorter path lengths in the image area, the photobleaching experienced in a CL implementation of PLIF (low laser intensity but long duration of illumination) is comparable to that in an LS implementation (high laser intensity but short duration of illumination).

In addition to path length considerations, several other factors can cause the analytical photobleaching model to produce a worst-case estimate of the extent of photobleaching in a PLIF configuration. For instance, pixels located in off-center portions of the image experience more diffuse illumination and therefore less photobleaching than predicted for pixels at the center of the image. Furthermore, observations of ''photobleaching recovery'' between subsequent scans (Saylor 1995; Sakakibara and Adrian 1999) indicate that the loss of fluorescence in a single scan/pass through the image area is likely dominated by quenching rather than irreversible photobleaching (Song et al. 1996), leading to recovery of the ground state between subsequent scans or photon absorption events. This recovery, in turn, leads to F^* values that are higher than predicted by the model for dye parcels exposed to multiple scans or with relatively long path lengths within the light sheet. As shown in the Experimental section, however, model predictions of photobleaching in the single-scan LS scenario are upheld by experimental results for typical laser intensities, beam diameters, and scan rates.

For values of the photobleaching constant greater than 0.2, the experimental data exhibited higher normalized fluorescence than was predicted by the analytical model (see Fig. 6). The deviations may be due to factors not accounted for by the model, such as multiphoton processes at long exposures (Lanni and Ware 1981; Sahar and Treves 1977), recovery of the ground state after quenching (i.e., ''photobleaching recovery''), or higher-order photobleaching kinetics (Song et al. 1996). However, the deviations are not of practical concern for most experiments, since they correspond to large-B situations where the photobleaching error is already unacceptably large. In the case of our experimental configuration, they also correspond to extremely long exposure times (5 s or longer) that greatly exceed the advective timescales of most experiments. Most experiments will be designed to have a value of B significantly less than 0.2 in order to avoid these errors, and the agreement between the experiments and analysis in this range is favorable. While the model presented in this paper is suitable for typical PLIF configurations, caution should be exhibited in extending the model to configurations with long exposure times, high laser intensities, and/or dye concentrations that exceed the tested range.

Overall, with the few caveats that we have discussed here (high-resolution PLIF configurations, long exposures, long path lengths in the light sheet), this model

indicates that fluorescein and other dyes with large $Q_b\sigma$ are acceptable choices for use in PLIF. This finding advances current knowledge of photobleaching in large-scale experimental fluid dynamics configurations. Some researchers (Cowen et al. 2001; Mead et al. 2003; Shiono and Feng 2003) have used Crimaldi's (1997) model for photobleaching in point-LIF configurations to estimate the extent of photobleaching in PLIF. Out of these, Mead et al. (2003) and Shiono and Feng (2003) decided, based on the analysis, to use Rhodamine 6G instead of fluorescein to avoid photobleaching. However, the difference in the extent of photobleaching predicted for point-LIF and PLIF geometries shows that the point-LIF analysis is not transferrable to PLIF geometry, and that, in cases where the extent of photobleaching in a point-LIF configuration is significant according to analytical model predictions, photobleaching is often negligible in the corresponding PLIF configuration, in which B is around two orders of magnitude lower. This conclusion is particularly favorable for some experimental fluids research; fluorescein is substantially cheaper than other dye alternatives and has some preferable chemical qualities (e.g., high quantum yield). Moreover, fluorescein has an absorption spectrum that is more blue-shifted than common dye substitutes (e.g., Rhodamine 6G), which could be advantageous for spectral separation when used in conjunction with other common dyes.

Acknowledgments This work is supported by the National Science Foundation under CAREER grant No. 0348855 to JPC and a Fannie and John May Hertz Foundation Fellowship to LGL. The authors thank two anonymous reviewers whose suggestions improved this work.

References

Borg A, Bolinder J, Fuchs L (2001) Simultaneous velocity and concentration measurements in the near field of a turbulent low-pressure jet by digital particle image velocimetry-planar laser-induced fluorescence. Exp Fluids 31:140–152

Brungart T, Petrie H, Harbison W, Merkle C (1991) A fluorescence technique for measurement of slot injected fluid concentration profiles in a turbulent boundary layer. Exp Fluids 11:9–16

Catrakis H, Dimotakis P (1996) Mixing in turbulent jets: scalar measures and isosurface geometry. J Fluid Mech 317:369–406

Coolen M, Kieft R, Rindth C, Steenhoven Av (1999) Application of 2-D LIF temperature measurements in water using a nd:yag laser. Exp Fluids 27:420–426

Coppeta J, Rogers C (1994) Mixing measurements using laser-induced fluorescence. Technical Report 95-0167, American Institute of Aeronautics and Astronautics

Coppeta J, Rogers C (1995) A quantitative mixing analysis using fluorescent dyes. Technical Report 96-0539, American Institute of Aeronautics and Astronautics

Cowen E, Chang K, Liao Q (2001) A single-camera coupled PTV-LIF technique. Exp Fluids 31:63–73

Crimaldi J (1997) The effect of photobleaching and velocity fluctuations on single-point LIF measurements. Exp Fluids 23:325–330

Crimaldi J, Koseff J (2001) High-resolution measurements of the spatial and temporal scalar structure of a turbulent plume. Exp Fluids 31:90–102

Crimaldi J, Wiley M, Koseff J (2002) The relationship between mean and instantaneous structure in turbulent passive scalar plumes. J Turb 3:1–23

Das C, Xia Z, Stoyanov A, Fan Z (2005) A laser-induced fluorescence imaging system for isoelectric focusing. Instr Sci Tech 33:379–389

Durst F, Schmitt F (1984) Joint laser-doppler/laser-induced fluorescence measurements in a turbulent jet. In: 2nd Symposium on applications of laser anemometry to fluid mechanics, Lisbon, Paper no. 8.5

Goldstein J, Smits A (1994) Flow visualization of the 3-dimensional, time-evolving structure of a turbulent boundary-layer. Phys Fluids 6:577–587

Guilbault G (1990) General aspects of luminescence spectroscopy. In: Guilbault G (eds) Practical fluorescence, 2nd edn. Dekker, New York, pp 1–40

Hishida K, Sakakibara J (2000) Combined planar laser-induced fluorescence-particle image velocimetry technique for velocity and temperature fields. Exp Fluids 29:S129–S140

Houcine I, Vivier H, Plasari E, Villermaux J (1996) Planar laser induced fluorescence technique for measurements of concentration in continuous stirred tank reactors. Exp Fluids 22:95–102

Imamura M, Koizumi M (1955) Irreversible photobleaching of the solution of fluorescent dyes. I. Kinetic studies on the primary process. Bull Chem Soc Jpn 28:117–124

Karasso P, Mungal M (1997) PLIF measurements in aqueous flows using the Nd:YAG laser. Exp Fluids 23:382–387

Koochesfahani M (1984) Experiments on turbulent mixing and chemical reactions in a liquid mixing layer. Ph.D. thesis, California Institute of Technology

Koochesfahani M, Dimotakis P (1985) Laser-induced fluorescence measurements of mixed fluid concentration in a liquid plane shear layer. AIAA J 23:1700–1707

Lanni F, Ware B (1981) Intensity dependence of fluorophore photobleaching by a stepped-intensity slow-bleach experiment. Photochem Photobiol 34:279–281

Lemoine F, Antoine Y, Wolff M, Lebouche M (1999) Simultaneous temperature and 2D velocity measurements in a turbulent heated jet using combined laser-induced fluorescence and LDA. Exp Fluids 26:315–323

Magde D, Wong R, Seybold P (2002) Fluorescence quantum yields and their relation to lifetimes of rhodamine B and fluorescein in nine solvents: improved absolute standards for quantum yields. Photochem Photobiol 75:327–334

Mead K, Wiley M, Koehl M, Koseff J (2003) Fine-scale patterns of odor encounter by the antennules of mantis shrimp tracking turbulent plumes in wave-affected and unidirectional flow. J Exp Biol 206:181–193

Munsterer T, Jahne B (1998) LIF measurements of concentration profiles in the aqueous mass boundary layer. Exp Fluids 25:190–196

Oster G, Adelman A (1956) Long-lived states in photochemical reactions. I. Photoreduction of eosin. J Am Chem Soc 78:913–916

Prasad R, Sreenivasan K (1990) Quantitative 3-dimensional imaging and the structure of passive scalar fields in fully turbulent flows. J Fluid Mech 216:1–34

Sahar E, Treves D (1977) Bleaching and diffusion of laser dyes in solution under high power UV irradiation. Opt Commun 21:20–24

Sakakibara J, Adrian R (1999) Whole field measurement of temperature in water using two-color laser induced fluorescence. Exp Fluids 26:7–15

Saylor J (1995) Photobleaching of disodium fluorescein in water. Exp Fluids 18:445–447

Shiono K, Feng T (2003) Turbulence measurements of dye concentration and effects of secondary flow on distribution in open channel flows. J Hydraul Eng 129:373–384

Smart P, Laidlaw I (1977) An evaluation of some fluorescent dyes for water tracing. Water Resour Res 13:15–33

Song L, Hennink E, Young I, Tanke H (1995) Photobleaching kinetics of fluorescein in quantitative fluorescence microscopy. Biophys J 68:2588–2600

Song L, Varma C, Verhoeven J, Tanke H (1996) Influence of the triplet excited state on the photobleaching kinetics of fluorescein in microscopy. Biophys J 70:2959–2968

Song L, Gijilswijk Rv, Yound I, Tanke H (1997) Influence of fluorochrome labeling density on the photobleaching kinetics of fluorescein in microscopy. Cytometry 27:213–223

Stapountzis H, Westerweel J, Bessem J, Westendorp A, Nieuwstadt F (1992) Measurement of product concentration of two parallel reactive jets using digital image processing. Appl Sci Res 49:245–259

Tian X, Roberts P (2003) A 3D LIF system for turbulent buoyant jet flows. Exp Fluids 35:636–647

Walker D (1987) A fluorescence technique for measurement of concentration in mixing liquids. J Phys E 20:217–224

Webster D, Roberts P, Raad L (2001) Simultaneous DPTV/PLIF measurements of a turbulent jet. Exp Fluids 30:65–72

Webster D, Rahman S, Dasi L (2003) Laser-induced fluorescence measurements of a turbulent plume. J Eng Mech 129(10):1130–1137

Westblom U, Svanberg S (1985) Imaging measurements of flow velocities using laser-induced fluorescence. Phys Scripta 31:402–205